INTERNATIONAL JOURNAL OF
NUMERICAL ANALYSIS AND MODELING
Volume 12, Number 2, Pages 254–267

ON THE COMPARISON OF PROPERTIES OF RAYLEIGH WAVES IN ELASTIC AND VISCOELASTIC MEDIA

YANGYANG HE, JINGHUAI GAO, AND ZHANGXIN CHEN

Abstract. Dispersion properties of Rayleigh-type surface waves are widely used in environmental and engineering geophysics to image and characterize a shallow subsurface. In this paper, we numerically study the Rayleigh-type surface waves and their properties in 2D viscoelastic media. A finite difference method in a time-space domain is proposed, with an unsplit convolutional perfectly matched layer (C-PML) absorbing boundary condition. For two models that have analytical expressions of wave fields/dispersion curves, we calculate their wave fields and compare the analytical and numerical solutions to demonstrate the validity of this method. For the case where a medium has a high Poisson's ratio, say 0.49, traditional finite difference methods with a PML boundary condition are not stable when modeling Rayleigh waves but the proposed method is stable. For a laterally heterogeneous viscoelastic media model (Model 1) and a two-layer viscoelastic media model (Model 2) with a cavity, we use this method to obtain their corresponding Rayleigh waves. For several quality factors, the dispersion properties of these Rayleigh waves are analyzed. The results of Model 1 show that in a shallow subsurface, the phase velocity of a fundamental mode of the Rayleigh waves increases considerably with a quality factor Q decreasing; the phase velocity increases with Poisson's ratio increasing. The results of Model 2 indicate that the energy of higher modes of the Rayleigh waves become strong when Q decreases.

Key words. Rayleigh waves, elastic and viscoelastic media, convolutional perfectly matched layer, stability, finite difference method.

1. Introduction

In most surface seismic surveys, a different frequency component of a surface wave has a different phase velocity. This dispersion property is of fundamental interest in oil exploration, engineering and environmental studies. Rayleigh waves were used to construct S-wave velocity profiles [20, 24, 25, 27, 28], study attenuation [6, 26] and investigate cavities in a shallow subsurface [11].

The Rayleigh waves can be simulated by solving wave equations through numerical methods. One of the most popular numerical methods is the finite difference method (FDM). Several approaches were applied at a free surface to model these Rayleigh waves in elastic media using the FDM [12, 16, 19, 30, 29]. In particular, the accuracy of heterogeneous staggered-grid finite difference modeling of the Rayleigh waves has been studied by [4].

In reality, inelasticity of earth materials has an important influence on wave propagation, particularly on surface waves. It is necessary to simulate Rayleigh waves and analyze their dispersion properties in viscoelastic media, for example. Several works [5, 10, 9] have studied the Rayleigh waves in a viscoelastic half-space. Andersion *et al.* [1] gave a relationship between Rayleigh wave attenuation coefficients and the quality factors Q_P and Q_S for P- and S-waves. Xia [26] inverted a quality factor Q from Rayleigh waves using this relationship. However, this relationship is based on a layered earth model, and it is difficult to deal with complex media

Received by the editors February 20, 2014.

2000 *Mathematics Subject Classification.* 35R35, 49J40, 60G40.

This research was supported by National Natural Science Foundation of China (40730424) and National Science & Technology Major Project (2011ZX05023-005).

such as laterally heterogeneous media. The finite difference method may be used in the study of such cases. The approaches applied to handle a free surface boundary condition in viscoelastic media are similar to those in elastic media. Carcione [6] presented Rayleigh waves forward modeling in linear viscoelastic media. Hestholm [14] studied finite difference modeling of seismic scattering from free-surface topography in 3D viscoelastic media. Saenger and Bohlen [23] described the application of a rotated staggered grid (RSG) to viscoelastic wave equations. However, these works did not study the effect of a quality factor Q on the dispersion properties of Rayleigh waves.

Absorbing boundary conditions are used to suppress reflections from the truncated edges of a model in the FDM. Bérenger [2] developed an absorbing boundary condition called the perfectly matched layer (PML) to attenuate electromagnetic waves. This PML has been extended to absorbing acoustic and elastic waves [8, 13, 17]. Komatitsch and Martin [15] introduced an unsplit convolutional PML (C-PML) to improve the behavior of the classical PML at grazing incidence. However, the classical FDM with PML and C-PML is not stable in Rayleigh waves modeling with a high Poisson's ratio of media [31].

In this paper, we study the effect of a quality factor Q on the Rayleigh waves in order to better understand their dispersion properties. We propose a finite difference method to simulate the Rayleigh waves in viscoelastic media. This method uses the RSG proposed by [22], which has less numerical dispersion. The validity of the method is demonstrated using two models that have an analytic solution. The C-PML absorbing boundary condition is used in this method. It is stable to absorb the Rayleigh waves with a high Poisson's ratio of media. With our accurate modeling method, we study the dispersion properties of the Rayleigh waves with different values of the quality factor Q in a shallow subsurface. These Rayleigh waves are calculated in two models, a laterally heterogeneous model and a two-layer model with a cavity. The results show that the Q in the near-surface has a strong effect on the dispersion properties of the Rayleigh waves, and it needs to be considered in the analysis of the Rayleigh waves in the real world. Our method is based on a 2D finite difference method in a time-space domain, which can be extended in a straightforward way to the 3D case.

2. The Method

In this section we introduce the wave equations in viscoelastic media, a free boundary treatment, and an absorbing boundary condition. A finite difference method is then developed, and its validity and stability are tested.

2.1. Wave equations. We use a second-order displacement-stress form of the viscoelastic wave equations in 2D. In a time-space domain, the equations are given by [7]:

$$\rho \ddot{u}_x = \frac{\partial \sigma_{xx}}{\partial x} + \frac{\partial \sigma_{xz}}{\partial z} + \rho f_x, \tag{1}$$

$$\rho \ddot{u}_z = \frac{\partial \sigma_{xz}}{\partial x} + \frac{\partial \sigma_{zz}}{\partial z} + \rho f_z, \tag{2}$$

$$\sigma_{xx} = (\lambda_u + 2\mu_u)\frac{\partial u_x}{\partial x} + \lambda_u \frac{\partial u_z}{\partial z} + (\lambda_r + \mu_r)\sum_{l=1}^{L_1} e_{1l} + 2\mu_r \sum_{l=1}^{L_2} e_{2l}, \tag{3}$$

$$\sigma_{zz} = (\lambda_u + 2\mu_u)\frac{\partial u_z}{\partial z} + \lambda_u \frac{\partial u_x}{\partial x} + (\lambda_r + 2\mu_r)\sum_{l=1}^{L_1} e_{1l} - \mu_r \sum_{l=1}^{L_2} e_{2l}, \tag{4}$$

$$\sigma_{xz} = \mu_u(\frac{\partial u_x}{\partial z} + \frac{\partial u_z}{\partial x}) + \mu_r \sum_{l=1}^{L_2} e_{3l}, \tag{5}$$

$$\dot{e}_{1l} = \Theta\Phi_{1l} - \frac{e_{1l}}{\tau_{\sigma l}^{(1)}}, l = 1, \ldots, L_1, \tag{6}$$

$$\dot{e}_{2l} = (\frac{\partial u_x}{\partial x} - \frac{\Theta}{2})\Phi_{2l} - \frac{e_{2l}}{\tau_{\sigma l}^{(2)}}, l = 1, \ldots, L_2, \tag{7}$$

$$\dot{e}_{3l} = (\frac{\partial u_x}{\partial z} + \frac{\partial u_z}{\partial x})\Phi_{2l} - \frac{e_{3l}}{\tau_{\sigma l}^{(2)}}, l = 1, \ldots, L_2, \tag{8}$$

$$\Theta = \frac{\partial u_x}{\partial x} + \frac{\partial u_z}{\partial z}, \tag{9}$$

$$\Phi_{vl} = \frac{1}{\tau_{\sigma l}^{(v)}}(1 - \frac{\tau_{\varepsilon l}^{(v)}}{\tau_{\sigma l}^{(v)}}), v = 1, 2, \tag{10}$$

where $\mathbf{x} = (x, z)$ are the Cartesian coordinates. $u_x(\mathbf{x}, t)$ and $u_z(\mathbf{x}, t)$ are the displacement components. $\sigma_{xx}(\mathbf{x}, t)$, $\sigma_{zz}(\mathbf{x}, t)$ and $\sigma_{xz}(\mathbf{x}, t)$ are the stress components. $\rho(\mathbf{x})$ denotes the density. $f_x(\mathbf{x}, t)$ and $f_z(\mathbf{x}, t)$ are the body forces. t is the time variable. $\ddot{u}_z$ is the second derivative of u_z with respect to time. $\lambda_u = (\lambda_r + \mu_r)M_{u1} - \mu_r M_{u2}$ and $\mu_u = \mu_r M_{u2}$ are the unrelaxed Lame constants, and λ_r and μ_r are the relaxed Lame constants. M_{uv}, $v = 1$, 2 are the relaxation functions evaluated at $t = 0$, with $v = 1$ being the dilatational mode and $v = 2$ being the shear mode. They are given by $M_{uv} = 1 - \sum_{l=1}^{L_v}(1 - \frac{\tau_{\varepsilon l}^{(v)}}{\tau_{\sigma l}^{(v)}})$, $v =$ 1,2. $\tau_{\varepsilon l}^{(v)}$ and $\tau_{\sigma l}^{(v)}$ are the material relaxation times. $e_{1l}(\mathbf{x}, t)$ are the memory variables related to the L_1 mechanisms which describe the viscoelastic characteristics of the dilatational wave, and $e_{2l}(\mathbf{x}, t)$ and $e_{3l}(\mathbf{x}, t)$ are the memory variables related to the L_2 mechanisms of the shear wave. The elastic case is obtained when $\tau_{\varepsilon l}^{(v)} \to \tau_{\sigma l}^{(v)}$, $\forall l$; then $M_{uv} \to 1$, $\Phi_{vl} \to 0$, and the memory variables vanish.

2.2. Free surface boundary. A rotated staggered grid (RSG) is used in our method. Figure 1 shows the locations of wavefield parameters and material parameters in the RSG. We assume that the free surface passes through the stress points. The stresses on the free surface are given by:

$$\sigma_{zz} = 0, \sigma_{xz} = 0. \tag{11}$$

Combining (11) with (4) and (5), we obtain

$$\frac{\partial u_z}{\partial z} = \frac{1}{\lambda_u + 2\mu_u}[\lambda_u \frac{\partial u_x}{\partial x} + (\lambda_r + 2\mu_r)\sum_{l=1}^{L_1} e_{1l} - \mu_r \sum_{l=1}^{L_2} e_{2l}], \tag{12}$$

$$\frac{\partial u_x}{\partial z} = -\frac{\partial u_z}{\partial x}, \tag{13}$$

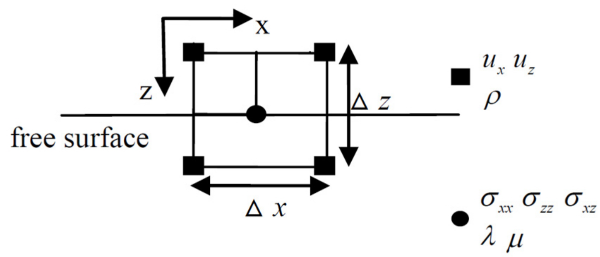

FIGURE 1. The distribution of modeling parameters within the rotated staggered grid (RSG). The stresses are placed at the filled circles; the displacements are placed at the filled rectangles. The free surface passes through the stress point.

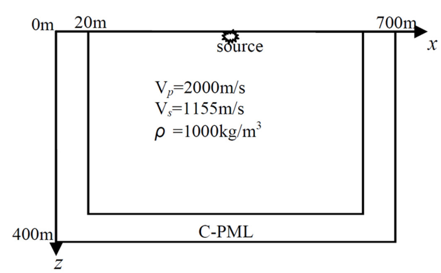

FIGURE 2. A sketch of the half-space homogenous model.

Then (3) can be written as

$$\begin{aligned}\sigma_{xx} &= (\lambda_u + 2\mu_u + \tfrac{(\lambda_u)^2}{\lambda_u+2\mu_u})\tfrac{\partial u_x}{\partial x} + (\lambda_r + \mu_r + \tfrac{\lambda_r+2\mu_r}{\lambda_u+2\mu_u})\sum_{l=1}^{L_1} e_{1l} \\ &+(2\mu_r - \tfrac{\mu_r}{\lambda_u+2\mu_u})\sum_{l=1}^{L_2} e_{2l}.\end{aligned} \tag{14}$$

In the numerical scheme, following [22], the derivatives are calculated along the 45°-rotated axes with respect to the Cartesian axes. We use a standard second-order centered time difference and a fourth-order Runge-Kutta space scheme.

In order to test the validity of our method, the Rayleigh waves are calculated for two models and compared with analytic solutions. Since there is no analytical solution for the Rayleigh waves in viscoelastic media in a time-space domain, the media considered in the two models are elastic. The first model is a half-space homogenous medium, see Figure 2. The C-PML is used in our method as the absorbing boundary condition, and it will be discussed in the next section. The thickness of C-PML is 20 m. The source is an impulse force in the vertical direction and is located at the middle of the domain ground; its time variation is a Ricker wavelet (15) with $t_0 = 0.05$ s and $f_0 = 20$ Hz:

$$h(t) = [1 - 2(\pi f_0(t - t_0))^2]exp[-(\pi f_0(t - t_0))^2]. \tag{15}$$

The finite difference grid size in the vertical and horizontal directions is $\triangle x = \triangle z = 2$ m, the time step is 0.1 ms and the total modeling time is 0.45 s. Figure 3 is the seismograms of one shot gather. The spacing distance between the adjacent receivers is 2 m. In the homogenous elastic medium, there is no velocity dispersion

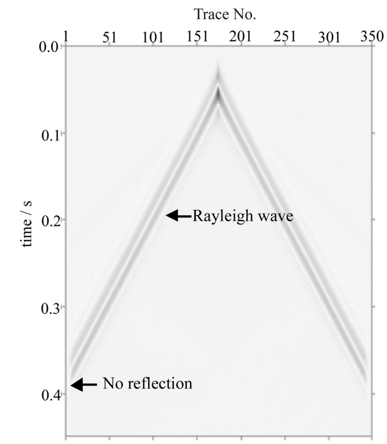

FIGURE 3. Vertical components of the Rayleigh wave in the half-space homogenous elastic medium.

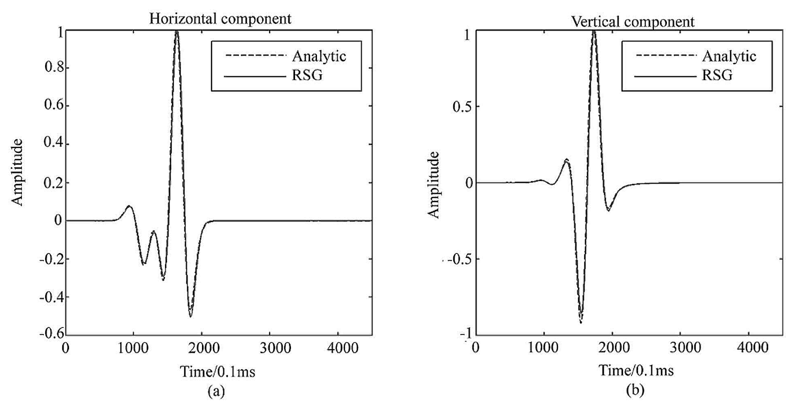

FIGURE 4. Seismograms (particle displacement) of analytical and numerical results; the offset is 120 m; (a) Horizontal component. (b) Vertical component.

in Rayleigh waves. Figure 4 compares the seismograms of our numerical result with the analytic solutions [3]; the offset is 120 m. The two seismograms are in good agreement. Our method performs well in the Rayleigh waves modeling.

The second model is a two-layer model, see Figure 5. The parameters are listed in Table 1. The thickness of C-PML is 10 m. The source is an impulse force in the vertical direction and is located on the ground, and its time variation is a Ricker wavelet (15), with $t_0 = 0.05$ s and $f_0 = 20$ Hz. The FD grid size is $\triangle x = \triangle z = 0.5$ m, the time step is 0.1 ms, and the total modeling time is 1 s. Figure 6 is a shot gather. The spacing distance between the adjacent receivers is 0.5 m. In the layered medium the dispersion of the Rayleigh waves occurs and higher mode Rayleigh waves are generated. In order to study the dispersion properties of these Rayleigh waves, computing the phase velocity of the Rayleigh waves is the standard analysis method used in most works. Park *et al.* [21] proposed a wavefield transformation method to construct the image of dispersion curves of the

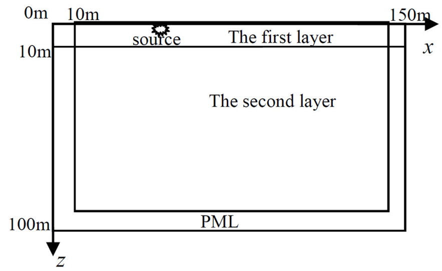

FIGURE 5. A sketch of two-layer model.

TABLE 1. Parameters of two-layer medium.

	z /m	ρ /(kg/m^3)	V_s /(m/s)	V_p /(m/s)
The first layer	10	2000	200	800
The second layer	90	2000	400	1200

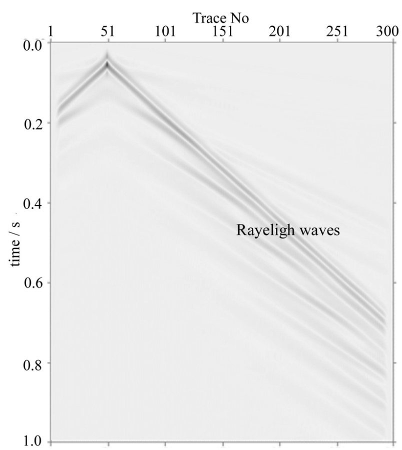

FIGURE 6. Vertical components of one shot seismograms in model 2.

Rayleigh waves. This method is used in our work. The image of these dispersion curves is shown in Figure 7(a). The dispersion curves of different modes are clearly identified. The phase velocities picked from the fundamental mode dispersion curve are compared with the theoretical values in Figure 7(b). The performance of our method is satisfactory.

2.3. Absorbing boundaries. The PML is now widely used in the modeling of wave propagation; however, it may have a problem in the Rayleigh wave modeling. The shallow earth material is complex; in particular, its Poisson's ratio is sometimes greater than 0.4. Zeng *et al.* [31] have studied the stability of the classical FD with PML and C-PML when modeling Rayleigh waves with a high Poisson's ratio of the medium by using numerical testing. They designed a half-space homogenous medium with Poisson's ratios varying from 0.10 to 0.49. The size of their 2D model is 50 m $\times$ 50 m and the thickness of PML is 10 m. The P-wave velocity is 520 m/s and the density is 1500 kg/m^3. The FD grid size is $\triangle x = \triangle z = 0.1$ m, the

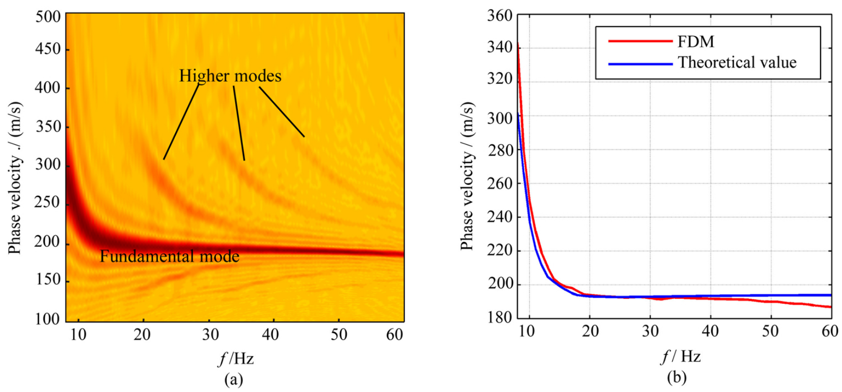

FIGURE 7. The image of dispersion curves of the Rayleigh waves in two-layer model. (a) Image of dispersion curves; (b) Dispersion curves. The red line is obtained from (a), and the blue line is the theoretical value.

time step is 0.05 ms, the maximum number of time loops is 40,000, and the total simulation time is 2 s. The FD with PML or C-PML would be considered stable if the simulation was completed without divergence. Zeng *et al.*'s work showed that the classical FD with both PML and C-PML is unstable if Poisson's ratio of the medium is greater than 0.39.

In this paper we use the C-PML in our FD method to model the Rayleigh waves in viscoelastic media. The efficiency of this absorbing boundary can be seen in Figure 3; there is no wave reflected from the absorbing boundary. We use the numerical testing shown above to study the stability of C-PML in our method. Here we define E as follows:

$$E(t) = \sum_x \sum_z |u_z(x, z, t)|. \tag{16}$$

It is a sum of the absolute value of u_z on every grid at each time. We model the Rayleigh wave propagation with Poisson's ratio γ varying from 0.46 to 0.49. The numerical results are shown in Figure 8. Our method have completed all the numerical tests without divergence. The FD with C-PML is stable with a high Poisson's ratio in our method. The difference between Zeng *et al.*'s method and our method is listed in Table 2. We use different differential equations and discretization grids. One speculation over the cause of the stability is that the dispersion relations for the RSG are independent of the Poisson's ratio.

The numerical tests and stability analysis above indicate that our method is an accurate and stable numerical method. With this method, we can model wave propagation with different parameters of media to better understand the properties of the Raleigh waves.

3. Numerical Results

In this section we simulate the Rayleigh wave propagation in two viscoelastic media to study the effect of a quality factor Q on the dispersion properties of Rayleigh waves.

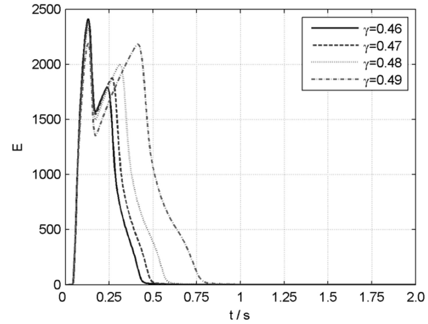

FIGURE 8. The value of E with different Poisson's ratio γ.

TABLE 2. The difference between Zeng *et al.*'s method and our method.

	Zeng *et al.*'s method	Our method
Equations	First-order velocity-stress form of the elastic wave equations	Second-order displacement-stress form of the viscoelastic wave equations
Grids	Madariaga-Virieux staggered grid	Rotated staggered grid
Stability	The classical FD with PML and C-PML is unstable	Our FD with C-PML is stable

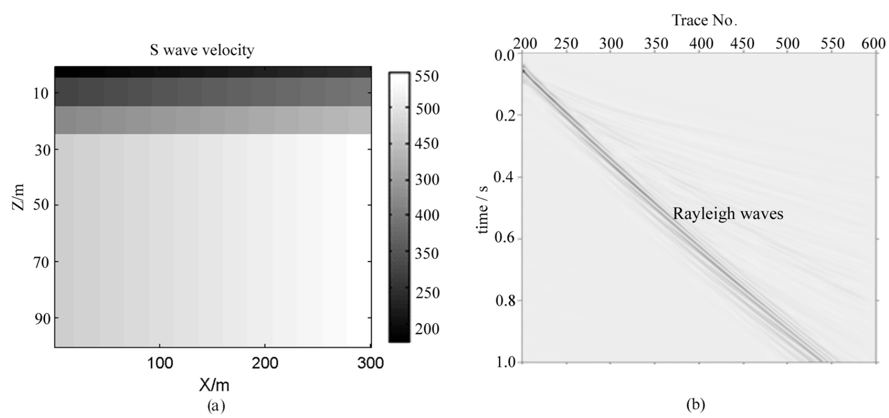

FIGURE 9. (a) The profile of V_S in Model 1; (b) the vertical component of single-shot seismograms.

3.1. Model 1: A laterally heterogeneous model. Model 1 is a laterally heterogeneous medium. The profile of S-velocity V_S is indicated in Table 3 and shown in Figure 9(a). The medium has four layers and V_S increases along the x-axis in each layer. The FD grid size is $\triangle x = \triangle z = 0.5$ m, the time step is 0.1 ms, and the total simulation time is 1 s. The source is an impulse force in the vertical direction and is located at (100 m, 0.25 m), and its time variation is a Ricker wavelet (15) with $t_0 = 0.05$ s and $f_0 = 20$ Hz. For simplicity, we make Q_S and Q_P equal in every layer; that is, $Q_S = Q_P = Q$.

TABLE 3. The V_S profile in Model 1.

z / m	5	10	10	75
V_S/ (m/s) x/ m	$150 + 0.5x$	$250 + 0.5x$	$350 + 0.5x$	$450 + 0.5x$

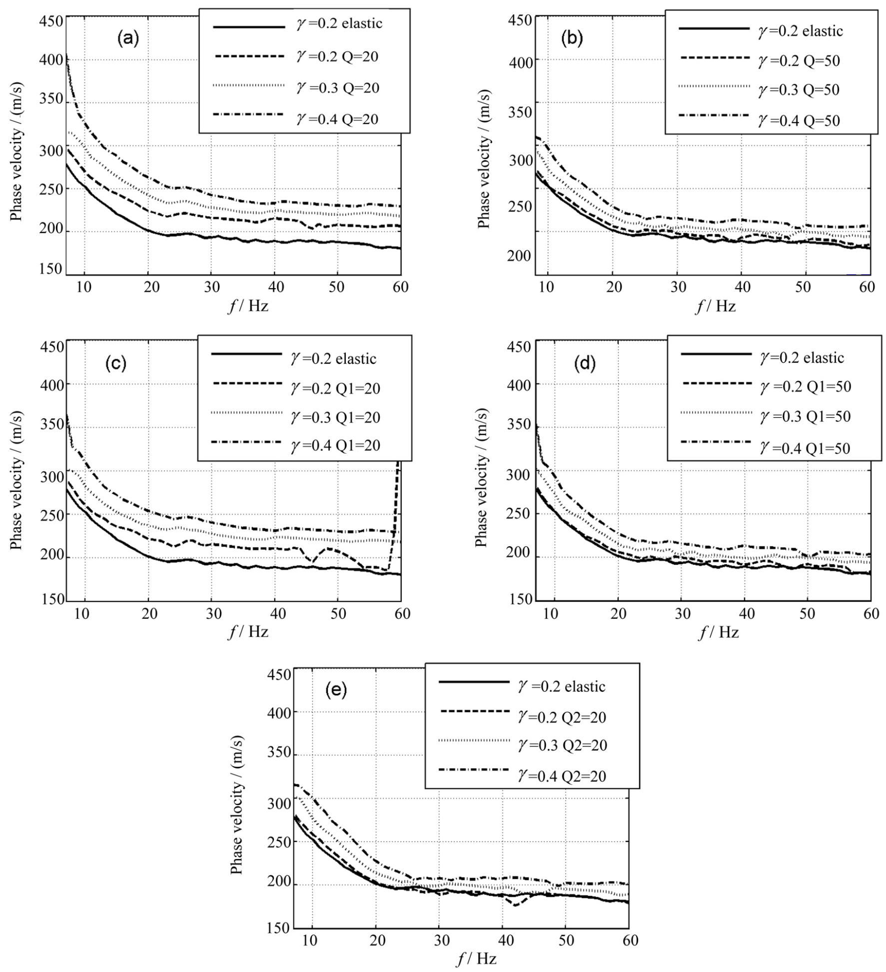

FIGURE 10. The dispersion curves with different parameters. (a) $Q_1 = Q_2 = Q_3 = Q_4 = Q = 20$; (b) $Q_1 = Q_2 = Q_3 = Q_4 = Q = 50$; (c) $Q_1 = 20$, $Q_2 = Q_3 = Q_4 = \infty$; (d) $Q_1 = 50$, $Q_2 = Q_3 = Q_4 = \infty$; (e)$Q_2 = 20$, $Q_1 = Q_3 = Q_4 = \infty$.

We now show the effects of Q and Poisson's ratio γ on the Rayleigh waves. First, when Q_1, Q_2, Q_3, and Q_4 in the four layers are changed and second, when Poisson's ratio γ is changed, we compute the dispersion curves of the fundamental mode Rayleigh wave and compare them with an elastic reference case. When we change Poisson's ratio γ, V_S remains constant and the velocity of P-wave is calculated according to γ.

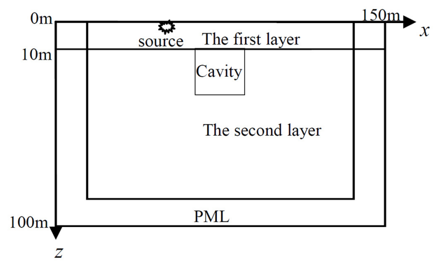

FIGURE 11. A sketch of Model 2.

The single-shot seismograms of Rayleigh waves in an elastic medium are shown in Figure 9(b). The spacing distance between adjacent receivers is 0.5 m. Figure 10 indicates the dispersion curves of the fundamental mode Rayleigh waves with different parameters of the medium. In Figure 10(a), the Q in the four layers are $Q_1 = Q_2 = Q_3 = Q_4 = 20$; in Figure 10(b), $Q_1 = Q_2 = Q_3 = Q_4 = 50$. In Figure 10(c), the Q in the first layer is $Q_1 = 20$ and the other layers are elastic media. In Figure 10(d), $Q_1 = 50$. In Figure 10(e), the first, third and fourth layers are elastic media, and the second layer is viscoelastic with $Q_2 = 20$. Poisson's ratio of the medium, γ, varies from 0.2 to 0.4 for each Q profile. The effects of Q and Poisson's ratio γ on the Rayleigh waves are concluded as follows:

1) For every frequency the phase velocity of the fundamental mode Rayleigh wave in a viscoelastic medium is higher than that of the fundamental mode Rayleigh wave in an elastic medium.

2) The phase velocity increases considerably with the quality factor Q_1 in the first layer but increases a little with the quality factor Q_2 in the second layer.

3) The higher Poisson's ratio, the higher the phase velocity.

3.2. Model 2: A two-layer model with cavity. Cavity detecting underground is important because it may lead to a natural or human-made hazard. Model 2 is a two-layer medium with a cavity, see Figure 11. The parameters for these two layers are listed in Table 1. The size of this square-shape cavity is 25 m $\times$ 25 m. A cavity of this size is observed sometimes in real world, such as a solution cavity. The cavity is located in the second layer with an S-wave velocity of 0.1 m/s, a P-wave velocity of 0.1 m/s and a density of 0.1 kg/m^3; the upper right vertex of this cavity is at position (62.5 m, 10 m). The source is located at (50 m, 0.25 m) and its time variation is a Ricker wavelet (15) with $t_0 = 0.05$ s and $f_0 = 20$ Hz. The size of the cavity is about 2 times that of the dominant wavelength of the Rayleigh waves; the cavity depth allows the smallest wavelength of these Rayleigh waves to propagate above it. The FD grid size is $\triangle x = \triangle z = 0.5$ m, the time step is 0.003125 ms, and the total simulation time is 1 s.

For simplicity, we make Q_S and Q_P in the first layer equal and assign to them three different values $Q_S = Q_P = Q = \infty$, 30, and 20. The seismograms of vertical displacement components are shown in Figure 12. A reflection pattern of the Rayleigh waves due to the cavity is clearly visible in these seismograms. Actually, some Rayleigh waves are reflected several times between the cavity and the soil surface. The dispersion images are shown in Figure 13. This figure clearly shows that the higher modes of the Rayleigh waves are involved; the energy of those higher modes of the Rayleigh waves becomes stronger when Q decreases. We note that there is a discontinuity in the image of the dispersion curve around $f = 23$

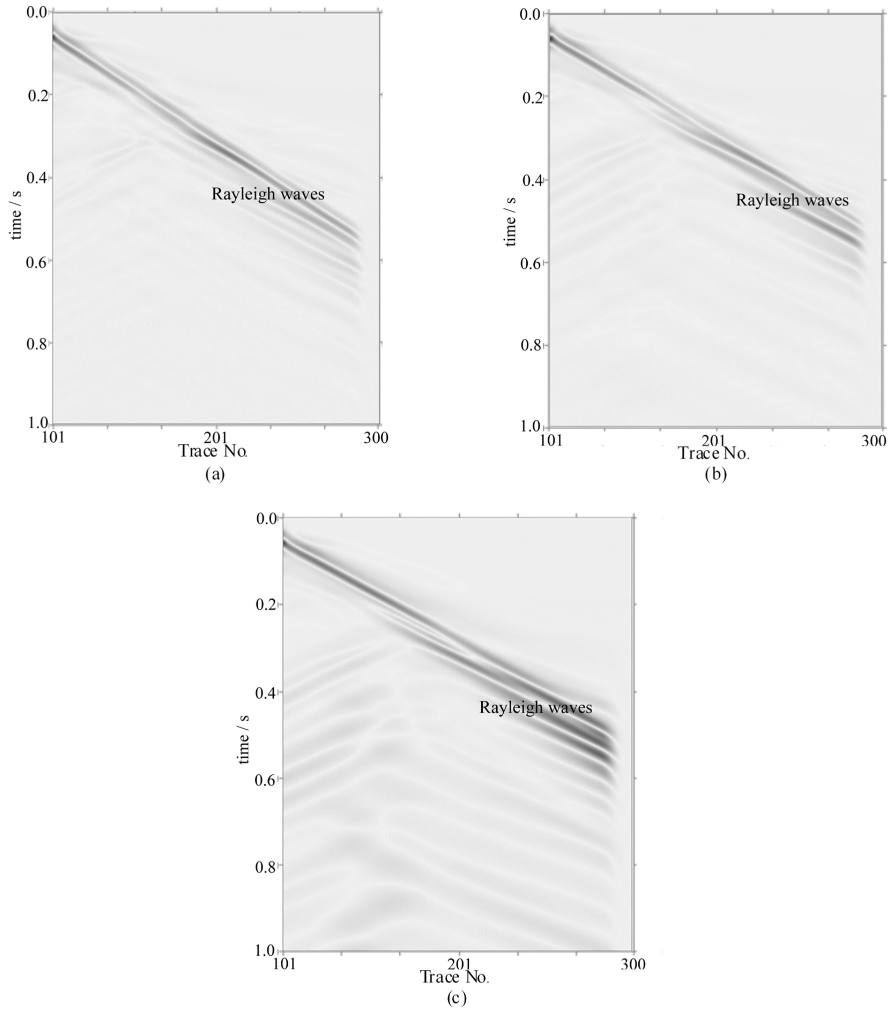

FIGURE 12. The seismograms of vertical displacement components in Model 2. (a) elastic medium; (b) $Q = 30$; (c) $Q = 20$.

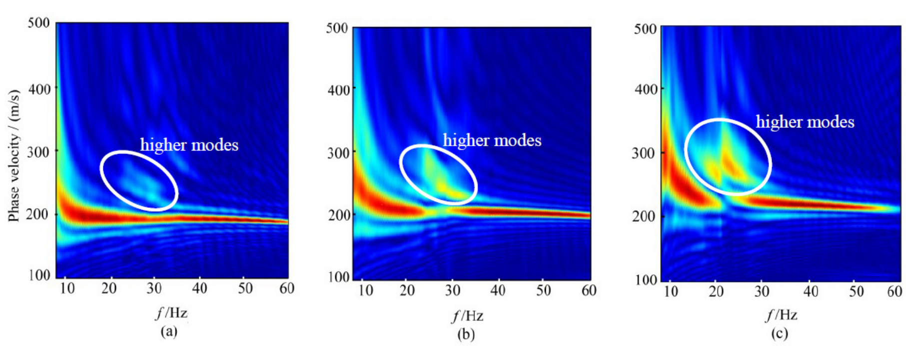

FIGURE 13. The images of dispersion curves of the Rayleigh wave in Model 2. (a) elastic medium; (b) $Q = 30$; (c) $Q = 20$.

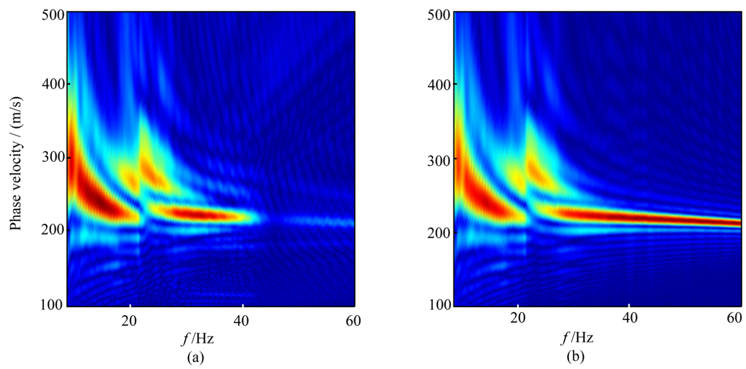

FIGURE 14. The images of dispersion curves of the Rayleigh waves in Model 2 with different centre frequency f_0 of the source. (a) $f_0 = 15$ Hz; (b) $f_0 = 30$ Hz.

Hz when $Q = 20$. The location of this discontinuity does not change when varying the centre frequency f_0 of the source, see Figure 14. Gelis *et al.* [11] studied the influence of the depth and size of a cavity on the dispersion curves of fundamental mode Rayleigh waves in elastic media. In viscoelastic media, the higher modes of Rayleigh waves have strong energy and can provide information for the parameters of the material underground in some practical applications. The influence of the depth and size of a cavity underground on the dispersion properties of higher mode Rayleigh waves in viscoelastic media will be investigated in further work.

4. Conclusions

We have proposed an accurate and stable 2D finite difference method to model Rayleigh waves in viscoelastic media. The C-PML in this method is stable when Poisson's ratio of the media is high. Using this method, the Rayleigh waves in complex media can be modeled to better understand the dispersion properties of these Rayleigh waves.

The wave propagations have been calculated in a laterally heterogeneous medium and a two-layer medium with a cavity with different values of Q. The dispersion properties of Rayleigh waves in viscoelastic media have been compared with those in the elastic case. Model 1 has shown that in a shallow subsurface, the phase velocity of the fundamental mode of the Rayleigh waves increases with Q decreasing and the phase velocity increases with Poisson's ratio increasing. The results of Model 2 have indicated that the energy of the higher modes of the Rayleigh waves become stronger when Q decreases. The difference of the Rayleigh waves between viscoelastic and elastic media shows that the Q in the near-surface should be considered in the analysis of the Rayleigh waves in the real world. Our method presented in this paper is based on 2D finite-difference modeling in a time-space domain. It will be developed in a 3D and surface topography case in further work.

References

[1] D.L. Anderson, A. Ben-Menahem and C.B. Archambeau, Attenuation of seismic energy in upper mantle. J. Geophys. Res., 70 (1965) 1441-1448.

[2] J. Brenger, A perfectly matched layer for the absorption of electromagnetic waves, J. Comput. Phys., 114 (1994) 185-200.

[3] P. Berg, F. If, P. Nielsen and O. Skovgaard, *Analytical reference solutions, Advanced seismic Modeling*. In Modeling the earth for oil exploration (ED. K. Helbig), p. 421-427, Pergamon Press, 1994.

[4] T. Bohlen and E. H. Saenger, Accuracy of heterogeneous staggered-grid finite-difference modeling of Rayleigh waves, Geophysics, 71 (2006) T109-T115.

[5] R. D. Borcherdt, Rayleigh-type surface wave on a linear viscoelastic half-space, J. Acoust. Soc. Am., 55 (1973) 13-5.

[6] J. M. Carcione, Modeling anelastic singular surface waves in the earth, Geophysics, 57 (1992) 781-792.

[7] J. M. Carcione, Seismic modeling in viscoelastic media, Geophysics, 58 (1993) 110-120.

[8] W. C. Chew and Q. Liu, Perfectly matched layers for elastodynamics: A new absorbing boundary condition, J. Comput. Acoust., 4 (1996) 341-359.

[9] P. K. Currie, M. A. Hayes and P. M. OLeary, Viscoelastic Rayleigh waves, Q. Appl. Math., 35 (1977) 35-53.

[10] P.K. Currie, Viscoelastic surface waves on a standard linear solid, Q. Appl. Math., 37 (1979) 332-6.

[11] C. Gelis, D. Leparoux, J. Virieux, A. Bitri, S. Operto and G. Grandjean, Numerical modeling of surface waves over shallow cavities, J. Environ. Eng. Geoph., 10 (2005) 111-121

[12] R. Graves, Simulating seismic wave propagation in 3D elastic media using staggered-grid finite difference scheme, B. Seismol. Soc. Am., 86 (1996) 1091-1106.

[13] F. D. Hastings, J. B. Schneider and S. L. Broschat, Application of the perfectly matched layer PML absorbing boundary condition to elastic wave propagation, J. Acoust. Soc. Am., 100 (1996) 3061-3069.

[14] S. Hestholm, Three-dimensional finite difference viscoelastic wave modeling including surface topography, Geophys. J. Int. 139 (2002) 852-878.

[15] D. Komatitsch and R. Martin, An unsplit convolutional perfectly matched layer improved at grazing incidence for the seismic wave equation, Geophysics, 72 (2007) 155-167.

[16] A. Levander, Fourth-order finite-difference P-SV seismograms, Geophysics, 53 (1988) 1425-1436.

[17] Q. Liu and J. Tao, The perfectly matched layer for acoustic waves in absorptive media, J. Acoust. Soc. Am., 102 (1997) 2072-2082.

[18] K. C. Meza-Fajardo and A. S. Papageorgiou, A nonconvolutional, split-field, perfectly matched layer for wave propagation in isotropic and anisotropic elastic media, Stability analysis, B. Seismol. Soc. Am., 98 (2008) 1811-1836.

[19] R. Mittet, Free-surface boundary conditions for elastic staggered-grid modeling schemes, Geophysics, 67 (2002) 1616-1623.

[20] S. Nazarian and K. H. Stokoe II, In situ shear wave velocities from spectral analysis of surface waves, 8th Conference on Earthquake Engineering, 3 (1984) 31-39.

[21] C.B. Park, R.D. Miller and J. Xia, Imaging dispersion curves of surface waves on multichannel record, 68th Annual International Meeting, Expanded Abstracts. SEG., pp: 1377-1380, 1998.

[22] E. H. Saenger, N. Gold and S. A. Shapiro, Modeling the propagation of elastic waves using a modified finite-difference grid, Wave Motion, 31 (2000) 77-92.

[23] E. H. Saenger and T. Bohlen, Finite-difference modeling of viscoelastic and anisotropic wave propagation using the rotated staggered grid, Geophysics, 69 (2004) 583-591.

[24] L. V. Socco, S. Foti and D. Boiero, Surface-wave analysis for building near-surface velocity models-Established approaches and new perspectives, Geophysics, 75 (2010) 75A83-75A102.

[25] J. Xia, R. D. Miller and C. B. Park, Estimation of near-surface shear-wave velocity by inversion of Rayleigh waves, Geophysics, 64 (1999) 691-700.

[26] J. Xia, R. D. Miller, C. B. Park and G. Tian, Determining Q of near-surface materials from Rayleigh waves, J. Appl. Geophys., 51 (2002) 121-129.

[27] J. Xia, R. D. Miller, C. B. Park and G. Tian, Inversion of high frequency surface waves with fundamental and higher modes, J. Appl. Geophys., 52 (2003) 45-57.

[28] J. Xia, Y. Xu, R. D. Miller and C. Chen, Estimation of elastic moduli in a compressible Gibson half-space by inverting Rayleigh wave phase velocity, Surv. Geophys., 27 (2006) 1-17.

[29] Y. Xu, J. Xia and R. D. Miller, Numerical investigation of implementation of air-earth boundary by acoustic-elastic boundary approach, Geophysics, 72 (2007) SM147-SM153.

[30] P. Moczo and F. Hron, Testing four elastic finite difference schemes for behaviour at discontinuities, B. Seismol. Soc. Am., 120 (1993) 663-676.

[31] C. Zeng, J. Xia, R. D. Miller and G. P. Tsoflias, Application of the multiaxial perfectly matched layer (M-PML) to near-surface seismic modeling with Rayleigh waves, Geophysics, 76 (2011) T43-T52.

National Engineering Laboratory for Offshore Oil Exploration, Institute of Wave and Information, School of Electronic and Information Engineering, Xi'an Jiaotong University, Xi'an 710049, China

E-mail: hyy1211@163.com and jhgao@mail.xjtu.edu.cn

Center for Computional Geoscience, Xi'an Jiaotong University, Xi'an 710049, China. Department of Chemical & Petroleum Engineering, University of Calgary, Calgary, AB T2N 1N4, Canada

E-mail: zhachen@ucalgary.ca